FABRICATION AND MODELING OF AN ANTHROPOMORPHIC ROBOTIC HAND WITH SENSORLESS GRASP FORCE ESTIMATION FOR USE OF PROSTHETIC WITH TACTILE FEEDBACK

[1]MANJU VIJAYAKUMAR SAROJAM, [2]DR.BHASKARAN UMAMAHESWARI, [3]DR.LATHA KARUNACHALA PANDIAN

College of Engineering, Guindy, Anna University, Chennai, India
E-mail: manju.vs1@gmail.com

Abstract - Developing an anthropomorphic robot hand to emulate movements of human hand for grasping tasks poses a significant challenge. Traditional designs of robotic manipulators resembling human hands face challenges in obtaining comprehensive feedback regarding the shape, texture, and physical attributes of grasped objects from actuators, sensors, and mechanical components. Existing approaches for controlling anthropomorphic hands relied on imitation, human demonstration, or predefined grasp types for control techniques. However, employing human demonstration for learning control strategies becomes impractical as the observation space expands and task intricacies grow, given the arduous and time-consuming nature of collecting demonstrations. Consequently, devising a controller for precise actuation and accurate force estimation becomes important. This research concentrates on fabricating or acquiring a lightweight and powerful artificial hand suitable for prosthetic use, emphasizing enhanced feedback through control systems and the prosthesis itself. In this study, a novel controller model is introduced, which incorporates computational intelligence (CI) technique through the Egret Swarm Optimization Algorithm (ESOA) to effectively tune the parameters of a Sliding Mode Estimator (SME). The simulation setup of this system is evaluated to demonstrate that this proposed feedback control strategy significantly minimizes estimation errors when compared to existing estimator models.

Keywords - Computational intelligence, Feedback Control, Metaheuristics, Robotic hand, Sliding Mode Estimator

I. INTRODUCTION

Human-robot interfaces have many applications such as prosthetics and artificial wrists (Yanco et al. 2015; Bajaj et al. 2019), manufacturing and industrial assembly lines (Lee et al. 2018), hand rehabilitation (Heung et al. 2019), surgery in medical robotic (Beasley, 2012), soft wearable robotics (Kang et al. 2019), assisted living and care (Malukas et al. 2018), drone based delivery (Ivanovas et al. 2018), territory patrolling (Luneckas et al. 2019), smart agriculture(Zhangetal.2020;Adenugbaetal.2019),militaryroboticsapplications(Sapaty, 2015), etc. However, accomplishing efficient object grasping and dexterous manipulation capabilities in robots remains an open challenge. While developing anthropomorphic hands of a robot, i.e., robotic manipulators that have a structure like the hands of a human (links and joints), it is challenging to accomplish feedback from actuators, sensors and mechanical part of the manipulators about shape, texture and other physical characteristics of the grasped object.

Grasping is considered as a fundamental skill that robots must practise before they can effectively replace numerous tasks handled manually by humans. The task of grasping by the robotic hands generally requires precise control actions with the help of tactile sensor feedbacks. The complexity involved in robotic manipulation tasks rises significantly when a gripper must devise viable techniques to address the challenges of grasping amidst potential uncertainties like unknown item properties or positions. In robotic hands, dexterous capabilities of grasping are conventionally performed through multi-joined, complex structures and sophisticated actuation mechanisms. Such hands are costly and hard to plan and develop and they require complex sensing and control. However, there exists one commonly assumed disadvantage of the usage of compliant hands: under actuation and passive compliance appear to provide difficulties in dexterous grasping or might even make it impossible. In the recent times, many researchers have attempted to construct under actuated hands using components that possess passive compliance.

These are simpler than traditional hands and because of under actuation, allow for simple control. Golan et al. (2021) introduced a versatile robot hand with an adaptable structure developed to accommodate a diverse array of objects. The adaption is guaranteed by restructuring the robot hand for performing desired grasping technique to grasp the previously unseen objects. Homberg et al. (2019) developed a soft hand for grasping effectively and recognize the objects shapes on the basis of the measurements of the states.

The internal sensors permit for hand configuration and the item to be detected. A clustering technique is used for recognizing ever grasped object in the presence of shape uncertainties of the item. Ji et al. (2019) connected vision along with robotic hand grasping control to accomplish accurate and reliable item being grasped in a complex clustered scene. Integration of sensor data enabled real-time control of grasping tasks, permitting the manipulation of diverse

objects with uncertain weights, stiffness, and friction characteristics. Kang et al. (2019) designed a unified gripper by integrating an under-actuated gripper with a suction-based system of gripping, enabling the grasp of a wide range of items across diverse environments.

Experiments utilizing a various range of objects falling under different grasping situations were implemented to exhibit the capability of grasping. Mu et al. (2020) developed a robot with a prototype of an end-effect or to pick kiwifruit, while its artificial fingers were mounted with fibre sensors to find the best position to grab the fruit without any damage. Neha et al. (2020) conducted the simulations on the grasping of 4-fingered robot hand to exhibit that the implemented hand of the robot has the ability to grasp objects of various shapes and sizes. Zhou et al. (2018) presented an intelligent strategy of grasping control for a customized 13-DOF based soft anthropomorphic robot hand. The hand was showcased for delivering efficient performance of grasping, ensuring safe and intelligent interactions even without stringent requirements on accuracy.

The most diffused control techniques depend on position control with force threshold, when the threshold is surpassed, the movement of finger is stopped even if the final position is not reached. These techniques not ensure a stable grasp and needs a preliminary knowledge of the objects to be controlled. A user needs to set a proper restraining force to prevent damaging the objects. More advanced control algorithm exploit the utilization of tactile sensors placed into phalanges of finger. Unfortunately, the tactile sensors are not always effectively integrable and compatible with hand controller.

Earlier works on controlling anthropomorphic hands has depended on imitation, human demonstration or predefined grasp types for control techniques. As the observation space becomes richer and the intricacy of task increases, utilizing the human demonstration for learning control techniques is not scalable, because collecting demonstration is known to be hard and tedious process. Practically, the designer might want to utilize simple and efficient controllers. Hence, the design of simple controller with little information of chaotic system still remain a problem. From this point of view, an evolutionary technique has inspired new designs and models. Numerous works has been has done using the evolutionary algorithm to solve the various problems. No study used the evolutionary algorithm for force estimation of an anthropomorphic robotic hand. In this study, an Egret Swarm Optimization Algorithm (ESOA) was used to tune the sliding model for the accurate force estimation. The main objectives of this study are;

- Fabricating or procuring a light weight and powerful artificial hand to be used as a prosthetic.
- Improving the feedback promoted by the control systems and the prosthesis itself and,as any other complex electronic commercial product, the reduction of cost and weight, maintaining or improving the quality.
- To adapt automatic estimation of actuation force, Sliding Mode Estimator (SME) is developed, whose gain parameters are tuned using a metaheuristic optimization algorithm called ESOA.

II. MATERIAL AND METHODOLOGY

The hand model was fabricated with three different materials such as steel, aluminium and Plastic – PLA using CATIA software. The finger is designed with two parts. The first and the second knuckle perform coordinated motion for most of the grasping. Sequentially they are connected byastraight solid barto givean under actuated mechanism. The first link isactuated withageared dc motorandthemotionis transmittedtothefirstknuckleby a worm gearsystem through ashaft. Themotor, the worm gear system, andthe finger shaftare supported bya plate.

The stress analysis with finite element analysis using ABAQUS software gives the strength of the finger as lower in 3 D printed finger breaking at a load of 7 N compared to steel finger and aluminium finger with yield stress at 14.38 N and 14.42 Nrespectively as shown in Figure1(a),1(b)and1(c).Steelhandissuitablefortasks requiringhighstrengthwhere weightisnot a constraint. Aluminium finger reduces the weight with approximately 35% reduction of yield strength. For use as prosthetic, most important criteria being easiness for user, weightreduction, easy maintenance and dexterity than strength 3 D printed PLA fingers have an advantage over metal fingers with 66% reduction of yield strength when compared to aluminium fingers.

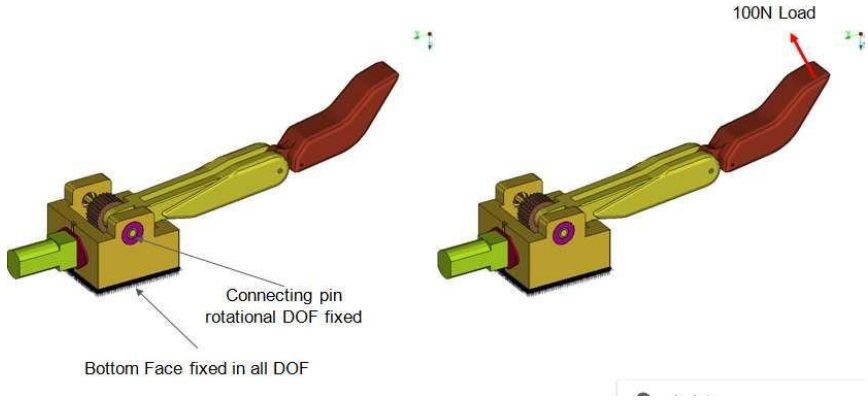


Figure1(a):StressanalysisontheroboticfingerinABAQUS



Figure 1(b): Stress plot of robotic finger with PLA material -Failure Load = 7 N Breaking Strain = 16.2 %

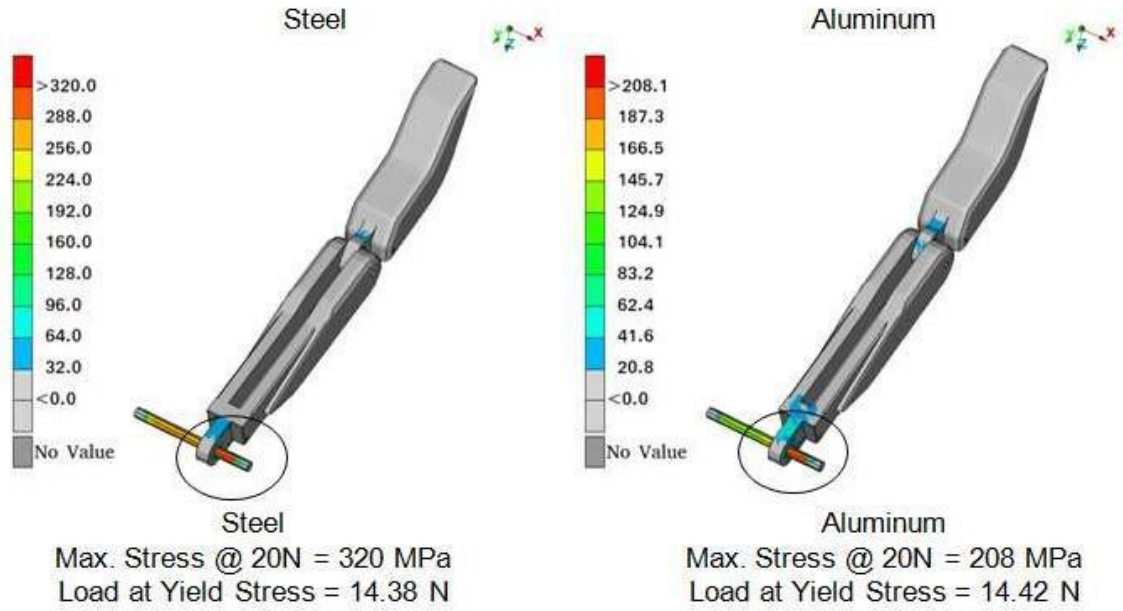


Figure 1(c): stress plot in steel finger **Figure 1(d): Stress plot in aluminium finger**

Figure 1: Strength analysis of the finger using ABAQUS software

Part	Material	Young's modulus(MPa)	Yield strength(MPa)	Breaking Strain(%)
RoboticFingers	Steel	206800	230	50
	Aluminum	69000	150	40
	Plastic–PLA	2526	51	16.2

Table1StrengthanalysisofroboticfingerinABAQUS

2.1Handarchitecture

Actuation is transmitted to the first link of the finger through spur gear and worm gear; and to thesecondlinkoffingerthroughabarlinkage.Figure2givestheexplodedviewofthefinger.

(1) Dc geared motor. (2) Base frame for the gears. (3) Worm gear which will rotate with the motor (4) Spur gear which transmits motion from the worm gear to the finger part (5) linkage that transmits motion to finger part (6), (7) finger links. At necessary regions roller bearings support the shaft

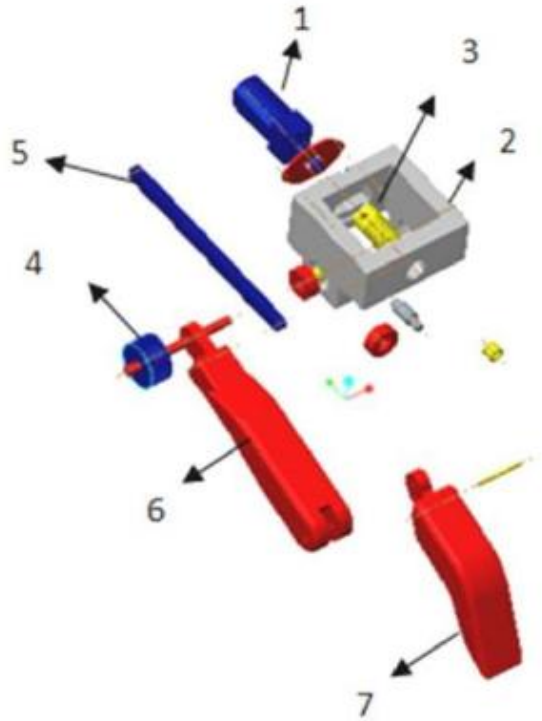


Figure2:Explodedviewofthefinger

Thedrafting iscustomized to thedimensions ofahuman hand. Micro Metal Gearmotor GA12N2060rpmisusedfor the designalong withencoder for position feedback[10].Ithas 4 Kg cm stall torque and it is light weight. Fused deposition modelling is used for additive manufacturing with PLA material [19]. 3 D printing parameters used are 0.16mm height and a printingspeedof50mm/s.Fingersandpalmwereprintedusing SLAwith 100%infill.Parts ofthe fingers wereassembled with 2mm shafts and fixed to the palm with4mm shaft. Bushings were fitted on MCP joints.Spur gears used are 16 teeth, 0.75 module, 6.11 degree right helical gearEN8material,3.5mmbore.Worm gears used arepinionOD8.5mm, 0.75modulethreads, helix angle 6.11 degree, bore 3.5 mm. The new palm design is shown in Figure 3. A similar fabrication with FDM technology of hand prosthesis consists of four moving fingers isdiscussed in [7]. Since our requirement was to move the fingers independently it wasredesigned with the help of an open source 3 D model in [1]. The difference from the design is that the gears were fabricated in metal in CNC. Also, thumbandpalm were redesigned.

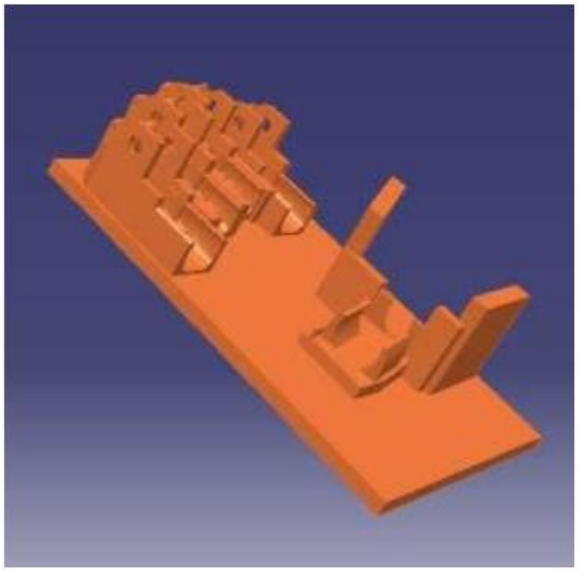


Figure.3Palmdesign

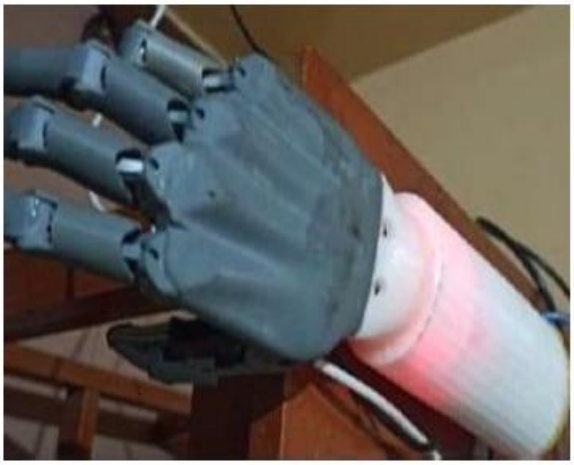


Figure.43Dprintedhandassembly

The thumb mechanism is modified to make it a single open and fold mechanism with better movement, agility and higher torque to grip and hold things. Spacers are placed in between the thumb base so that the base spur gear does not slip away from the worm gear. Complete hand after assembly is showninFigure4. Therobotic handelectronics are embeddedinacustomized PCB located in the palm. Figure 5 demonstrates the schematic of the control system. It includes the motor drivers(ThreeL9110dualchannelmotor drivers),the currentsensors (ACS712), and power regulation ICs (Integrated Circuits).

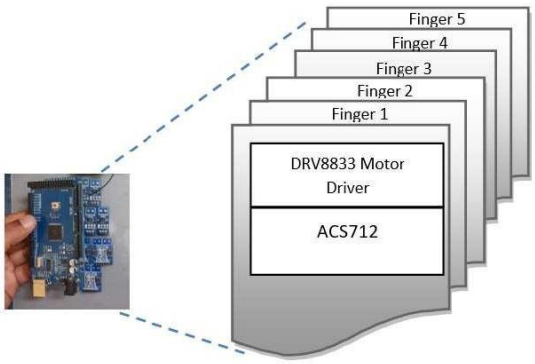


Figure.5TestingoftheFingersandPCB

III. PROPOSED EGRET SWARM OPTIMIZATION ALGORITHMTUNED SLIDING MODEL ESTIMATOR (ESOA-SME)

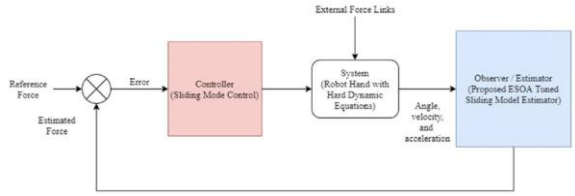


Figure.6 Proposed Architecture

The ESOA was used for the parameter optimization problem. Here, gain of guidance command wasobtainedbyconvertingtheguidancelawdesignprobl emtoparameteroptimization

problem. An SME is used to determine the line of straight angle rate for which the law of guidancewasrequired.Basedonthe Lynapunovtheory,theguidancelawcanbeconverging to zero, which is proved. The proposed ESOA method optimally selects the suitable gain parameters k and m of the sliding mode estimator.

3.1 Kinematics

Designed hand represents a kinematic chain with multiple links connected by revolute joints in series. One end linked with a fixed base and the other end is free. Hand is considered having 5 kinematic chains, F1, F2, F3 and F4 which are the four fingers in the hand and F5 is the thumb. f1isfirstfingerlinklengthandf2issecondlinklength, θlisfirstlinkangle and θ2issecond link angle.Thebarconnectedbetweenjoint1 andjoint2makeslinkf2moverelativetolink f1 through an angle of θ2 α θl. θfis the angle corresponding to each finger with respect to reference. Table 2 gives the DenavitHartenberg values at each joint. l is the finger length from the base joint.

Joint	θ_i	α_i	a_i	d_i
1	θ_f	θ_f	0	0
2	θ_l	0	fl	0
3	θ_u	0	f2	0

Table2: Denav it Hartenberg Table for Fingers

Thekinematicequationsofthefingersareobtainedas

$$x=(l+f_l\cos\theta_l+f_u\cos(\theta_l+\theta_u))*cos\theta_f \quad (1)$$

$$y=(l+f_l\sin\theta_l+f_u\sin(\theta_l+\theta_u))*sin\theta_f \quad (2)$$

$$z=f_l\sin\theta_l+\sin(\theta_l+\theta_u) \quad (3)$$

Thekinematicequationsarewrittenfor$\theta_1$and$\theta_2$movingindependently.

DHtransformationmatrixforadjacentframespandp-1asexplainedin[15]is:

$$A_p^{p-1}=\begin{bmatrix}\cos\theta_p & -\cos\alpha_p\sin\theta_p & \sin\alpha_p\sin\theta_p & a_p\cos\theta_p \\ \sin\theta_p & \cos\alpha_p\cos\theta_p & -\sin\alpha_p\cos\theta_p & a_p\sin\theta_p \\ 0 & \sin\alpha_p & \cos\alpha_p & d_p \\ 0 & 0 & 0 & 1\end{bmatrix} \quad (4)$$

Here p =4

3.2 Dynamics

Applying Lagrangian Euler formulation to the Lagrangian function, the necessary generalized torques τ_p for joint p actuator to drive the p[th] link of the finger is given by:

$$\tau_p = \frac{d}{dt}\left(\frac{\partial L}{\partial \dot{q_p}}\right) - \frac{\partial L}{\partial q_p} \quad (5)$$

Where q is the angle of the link and t is the time and Lagrangian function, L is the sum of kinetic energy (K) and potential energy (P).

Substituting the equations for K and P in L and finding the torque we get

$$\tau_p = \sum_{k=1}^{n} D_{pk}\ddot{q_k} + \sum_{k=1}^{n}\sum_{m=1}^{n} h_{pkm}\dot{q_k}\,\dot{q_m} + G_p \quad (6)$$

where p = 1, 2…, n for n joints.

D_{pk} is inertial acceleration

$h_{pkm}$is non linear corialis and centrifugal force vectors

G_p is gravity loading force vector

$$D_{pk} = \sum_{a=\max(p,k)}^{n} Tr\left[d_{ak} I_a d_{ap}^T\right] \quad (7)$$

$$I_p = \begin{bmatrix} \frac{1}{2}(-I_{xx}+I_{yy}+I_{zz}) & I_{xy} & I_{xz} & m_i x_i \\ I_{xy} & \frac{1}{2}(-I_{xx}+I_{yy}+I_{zz}) & I_{xy} & m_i y_i \\ I_{xy} & I_{xy} & \frac{1}{2}(-I_{xx}+I_{yy}+I_{zz}) & m_i z_i \\ m_i x_i & m_i y_i & m_i z_i & m_i \end{bmatrix} \quad (8)$$

$$G_i = -\sum_{p=i}^{n} m_p g d_{pi} \quad (9)$$

$$d_{ij} = \left\{A_{j-1}^{0} Q_j A_i^{j-1}\right\} \text{ for } j \le i \quad (10)$$

$$= 0 \; for \; j > i$$

For a single finger

$$D_{ll} = \left(\frac{1}{3}m_l + m_u\right) * l_l^2 + \frac{1}{3}m_u l_u^2 + m_u l_l l_u \cos(\theta_u) \quad (11)$$

$$D_{lu} = m_u\left(\frac{1}{3}l_u^2 + \frac{1}{2}(l_l l_u cos(\theta_u))\right) \quad (12)$$

$$D_{ul} = D_{lu} \quad (13)$$

$$D_{uu} = \frac{1}{3}m_u l_u^2 \quad (14)$$

$$D = \begin{bmatrix} D_{ll} & D_{lu} \\ D_{ul} & D_{uu} \end{bmatrix} \quad (15)$$

$$h_{ijk} = \sum_{p=\max(i,j,k)}^{n} Tr\left[\frac{\partial d_{pk}}{\partial q_p} I_p d_{pi}^T\right] \quad (16)$$

$$H_l = -m_u l_l l_u sin\theta_u \dot{\theta}_l \dot{\theta}_u - .5\, m_u l_l l_u sin\theta_u \dot{\theta}_l^{\,2} \quad (17)$$

$$H_u = .5\, m_u l_l l_u \cos(\theta_l + \theta_u)\dot{\theta}_l^{\,2} \quad (18)$$

$$H = \begin{bmatrix} H_l \\ H_u \end{bmatrix} \quad (19)$$

$$G_l = (0.5m_l + m_u) l_l cos\theta_l + .5\, m_u l_l l_u \cos(\theta_l + \theta_u) * 9.81 \quad (20)$$

$$G_u = .5\, m_u l_u \cos(\theta_l + \theta_u) * 9.81 \quad (21)$$

$$G = \begin{bmatrix} G_l \\ G_u \end{bmatrix} \quad (22)$$

$$\ddot{\theta} = D^{-1}\left[\left[V * \frac{k_m}{r}\right] - [H + G] - F_f\right] \quad (23)$$

$F_{f=\, frictional\ force\ proportional\ to\ velocity}$

Estimated current, $i_e = \frac{V - k * \dot{\theta}}{r}$ (24)

Where k and r are motor parameters

If measured current is i, $\delta = i - i_e$ (25)

$$sliding\ variable, s = k_p * \delta + k_d * \dot{\delta} + k_i * \int \delta \quad (26)$$

Where k_p, k_d and k_i are proportional derivative and integral error constants

The primary idea is to bring and keep the errors on a sliding surface such that the system is insensitive to disturbances and parameters changes (Yagiz *et al.* 1997).

The following is the final equation arrived for force estimation:

Force estimate, $\varphi_f = k * \delta + m * sgn(s)$ (27)

where k is the control gain, δ is the reference value, and m is the slope/rate constant.

Different values of k and m yield different control outputs. Hence, to find the optimal values of k and m, the proposed methodology introduces ESOA for tuning.

3.3. Modelling Egret Swarm Optimization Algorithm fortuning SME

Zuyan Chen et al. (2022) introduced an Egret Swarm Optimization Algorithm (ESOA), which was inspired by the predatory nature of the snowy egrets and great egrets. The egret indicates the collection offourbird species such asgreat egret, middle egret, littleegret and yellowbilled egret, which are all known for their magnificent white plumage. Most of the egrets inhibit coastal islands, rivers, lakes, ponds, rice paddies, streams, estuaries and marshlands closer to their shores. They are typically seen in pairs or in small groups (Kent, 1986; Dimalexis*et al.* 1997; Wiggins, 1991). The great egrets that possess aggressive system of search have theability to balance high consumption of energy for greater returns (Maccarone et al. 2012). ESOA comprises of 3 major phases such as sit and wait approach, aggressive approach and discriminant conditions as shown in figure 6. Egret populations (possible values of k and m) comprises of *n* groups of egret teams, where every egret team contains three egrets.Egret A appliesthesit andwaitapproach, egretB andCembrace therandomizedwalkandencirclement technique in the aggressive approach.

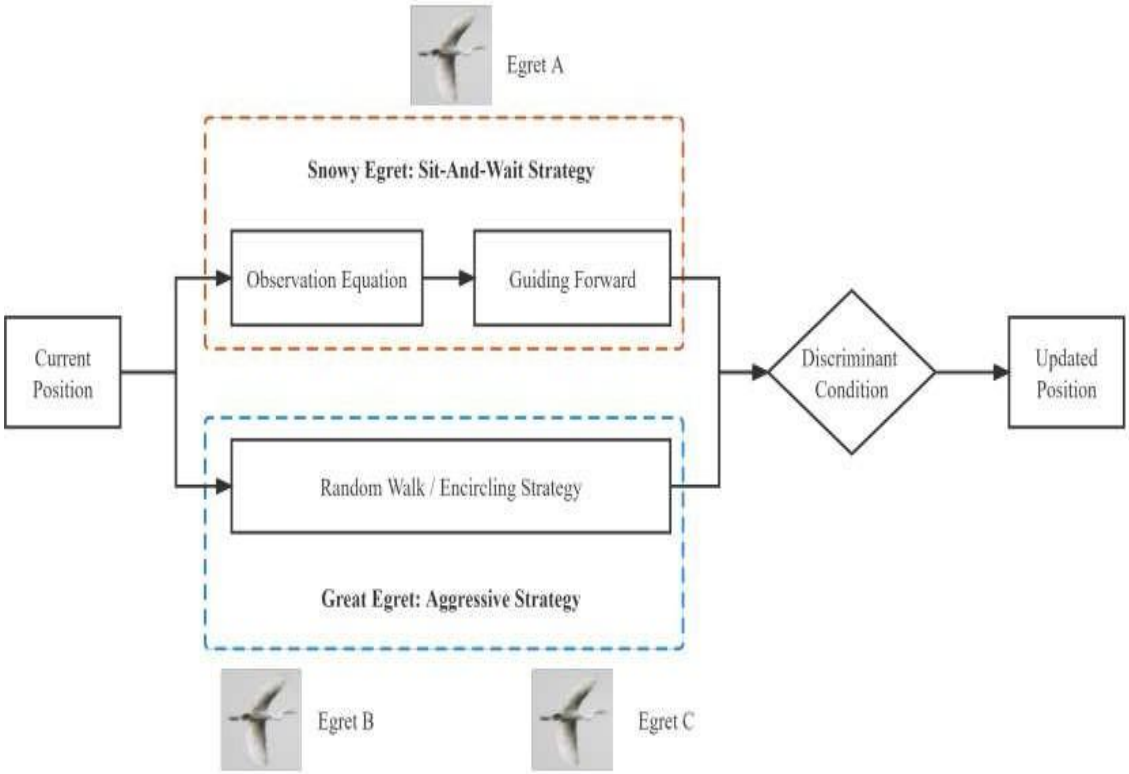


Figure. 6 Flow diagram of ESOA
[Source:ZuyanChenetal.(2022)]

The idea is to tune the values of k and m using Computational Intelligence (CI) algorithm through ESOA, which a latest metaheuristic algorithm, that can be used to automatically search for the optimal gain values of k and m that minimize a fitness function. The fitness function is defined based on the performance specifications and constraints of the robotic system. In this case, the Integral Absolute Error (IAE) function is considered as the fitness function.

2.2.1 Sit and wait strategy

The observation equation of the i^{th} Egret A was given by $\hat{y}_i = E(x_i)$, E indicates the evaluation method of Erget A for possible targets at the current area, x_i indicates the position (set of values of k and m) of group i. Determine the current estimate value of prey $\hat{y}_i$ by iteration and determine the e_i.

$$\hat{y}_i = w_i * x_i \tag{28}$$

$$e_i = \frac{\|\hat{y}_i - y_i\|^2}{2} \tag{29}$$

w_i denotes the weight of evaluation method; * is the multiplication; $\hat{g}_i$ is the practical gradient of w_i. The $\hat{g}_i$ was calculated using the partial derivative of e_i.

$$\hat{g}_i = \frac{\partial e_i}{\partial w_i} = \frac{\partial \|\hat{y}_i - y_i\|^2 / 2}{\partial w_i} = (\hat{y}_i - y_i) * x_i \tag{30}$$

$$\hat{d}_i = \frac{\hat{g}_i}{|\hat{g}_i|} \tag{31}$$

w_i is a matrix randomly generated according to uniform distribution. $w_i$is updated using a random algorithm;

$$m_i = \beta_1 * m_i + (1 - \beta_1) * g_i \tag{32}$$

$$v_i = \beta_2 * v_i + (1 - \beta_2) * g_i^2 \tag{33}$$

$$w_i = w_i - m_i / \sqrt{v_i}\ \mathrm{v} \tag{34}$$

The objective or fitness function defined to evaluate the optimality of the egret population (k and m) can be formulated using IAE as expressed below.

$$f_i(k, m) = \int_0^T e(t)dt \tag{35}$$

The value of β_1 and β_2 is 0.9 and 0.99; the initial value for m_t and v_t are set as 0; $\vec{d}_t$ indicates the direction of egret flight. The egret will draw on experience of two predication direction of egrets, they are: (1) the direction revision of best position of current egret population ($d_{h,i}$) and (2) the direction revision of best position in the overall population ($d_{g,i}$).

$$d_{h,i} = \frac{x_{ibest} - x_i}{|x_{ibest} - x_i|} * \frac{f_{ibest} - f_i}{|x_{ibest} - x_i|} + d_{ibest} \quad (36)$$

$$d_{g,i} = \frac{x_{gbest} - x_i}{|x_{gbest} - x_i|} * \frac{f_{gbest} - f_i}{|x_{gbest} - x_i|} + d_{gbest} \quad (37)$$

where d_{ibest} is the direction of flight of best egret in the team; d_{gbest} is the flight direction of best individual in egret population; x_{ibest} is the optimal value of egret team and population; f_{ibest} and f_{gbest} are the best fitness values found in the egret team and the overall population, respectively. The pseudo gradient of weight in observation equation was calculated using the equation;

$$g_i = \left(1 - r_h - r_g\right) * \vec{d}_t + r_h * d_{h,i} + r_g * d_{g,i} \quad (38)$$

where $r_h, r_g \in [0, 0.5]$, the updated position of egret A is given as;

$$x_{a,i} = x_i + \exp\left(\frac{-t}{0.1 * t_{max}}\right) * 0.1 * hop * g_i \quad (39)$$

where t is the current search iteration; t_{max} is the maximum count of iteration; hop is the D-value of position boundary which implies that value of hop is equal to upper limit of solution minus lower limit of solution.

2.2.2 Aggressive strategy

The aggressive strategy was employed by egret B is called as the random walk. The energy consumption of random walk was high; however, egret B is likely to get higher benefits. The updated position of egret B is as follows;

$$x_{b,i} = x_i + tan(r_{b,i}) * \frac{hop}{1+t} \quad (40)$$

where $x_{b,i}$ is the random number in $(^{\pi}/_{2}, ^{\pi}/_{2})$.

Egret C embraces the encirclement methodology. When it finds its prey, it will pursue it until it is caught.

$$D_h = x_{ibest} - x_i \quad (41)$$

$$D_g = x_{gbest} - x_i \tag{42}$$

$$x_{c,i} = \left(1 - r_i - r_j\right) * x_i + r_i * D_h + r_j * D_g \tag{43}$$

where D_h is the difference matrix between current an optimal position of egret group; D_g is the difference matrix between current an optimal position of egret population; r_i and r_j are random number in [0, 0.5].

2.2.3 Discriminant condition

After every egret in the egret group computes the updated position, they will conjointly determine the updated position of egret team. The solution matrix is as follows;

$$x_{s,i} = [x_{a,i}, x_{b,i}, x_{c,i}] \tag{44}$$

The egret team compares the updated position and fitness of three egrets with that of the preceding iteration. If one egret revised position is better than the preceding iteration, it will retain the update. If the updated position of all egret are worse than the previous iteration, there is a 30% probability to use the scheme with the worse update position. Thus the final solution set gives the final optimal values of k and m for the SME.

4. Results and Discussion

The proposed system with the novel control strategy is evaluated in MATLAB/SIMULINK R2020a environment. The performance of the proposed ESOA-SME is validated against the existing SME model, and SME tuned by two popular classical metaheuristic algorithms called Genetic Algorithm (GA) and Particle Swarm Optimization (PSO).

Figure 7 shows the characteristics of actual force and the force estimated by 4 control models, namely, SME, PSO-SME, GA-SME, and the proposed ESOA-SME. It can be observed that, the force estimated by the proposed ESOA-SME is more likely to follow the pattern of the actual force with a minimal variation. On the other hand, the force estimated by the rest of the 3 models shows larger variations from the actual force comparatively.

Furthermore, the error measurements of the force like absolute error, Mean Absolute Error (MAE), Mean Square Error (MSE), and Root Mean Squared Error (RMSE) are taken for comparison as follows.

Figure 8 shows the error values obtained for the 4 models. It is evident that the error produced by ESOA-SME is found to be least compared to the other 3 models with the values ranging

from -2.96 to 14.39882 with a mean of 5.32956. Error obtained by GA-SME is found to be the next better model with the values ranging from -0.0964 to 62.4749 with a mean of 22.19358. Error obtained by PSO-SME is found to be more than the GA-SME with values ranging from -0.1571 to 61.02847 with a mean of 32.26794. Error obtained by SME is found to be the highest with values ranging from -0.15692 to 62.29472 with a mean of 39.24176.

MAE is a measure used to quantify the accuracy of the estimator by measuring the average absolute differences between predicted and actual values in a dataset. MAE can be described in the following manner,

$$MAE = \frac{1}{n}\left(\sum_{i=1}^{n} | f_{actual} - f_{estimate} |\right) \quad (45)$$

Where, f_{actual} is the actual force, $f_{estimated}$ is the estimated force, and n is the number of instances.

Figure 9 shows the MAE values obtained for the 4 models. It is evident that the MAE produced by ESOA-SME is found to be least compared to the other 3 models with the values ranging from 0 to 579.2453 with a mean of 215.7599. MAE obtained by SME is found to be the next better model with the values ranging from 0 to 3924.2811 with a mean of 1395.3601. MAE obtained by PSO-SME is found to be more than the SME with values ranging from 0 to 14885.7582 with a mean of 4748.0274. MAE obtained by GA-SME is found to be the highest in this case, with values ranging from 0 to 15893.56635 with a mean of 5074.0167.

MSE is a measure used to quantify the accuracy and goodness of fit of a predictive model or estimator. It evaluates the mean of the squared differences between estimated and actual force values. The squared differences penalize larger errors more heavily compared to the smaller ones. MSE can be expressed as follows,

$$MSE = \frac{1}{n}\left(\sum_{i=1}^{n} (f_{actual} - f_{estimated})^2\right) \quad (46)$$

Figure 10 shows the MSE values obtained for the 4 models. It is evident that the MSE produced by ESOA-SME is found to be least compared to the other 3 models with the values ranging from 0 to 4608.2031 with a mean of 1629.64215. MSE obtained by SME is found to be the next better model with the values ranging from 0 to 198561.7895 with a mean of 60269.5475. MSE obtained by PSO-SME is found to be more than the SME with values ranging from 0 to 3103548.614 with a mean of 754360.4902. MSE obtained by GA-SME is found to be the highest in this case, with values ranging from 0 to 3533036.025 with a mean of 845521.3701.

RMSE is a measure used to evaluate the accuracy and performance of the control model. It is essentially the square root of the MSE, providing a more interpretable measure of the average error between estimated and actual values of force. RMSE can be expressed as follows,

$$RMSE = \sqrt{MSE} \tag{47}$$

Figure 11 shows the RMSE values obtained for the 4 models. It is evident that the RMSE produced by ESOA-SME is found to be least compared to the other 3 models with the values ranging from 0 to 67.8837 with a mean of 32.6718. RMSE obtained by SME is found to be the next better model with the values ranging from 0 to 445.6027 with a mean of 196.3555. MSE obtained by PSO-SME is found to be more than the SME with values ranging from 0 to 1761.6891 with a mean of 672.7056. MSE obtained by GA-SME is found to be the highest in this case, with values ranging from 0 to 1879.6372 with a mean of 715.4583.

Thus, from the comparative analysis it can proved that the proposed ESOA-SME model performs better estimation of force compared to SME, PSO-SME, and GA-SME. Data cannot be shared openly but are available on request from authors.

5. Conclusion

This research work focused on fabricating a lightweight prosthetic robotic hand with enhanced feedback control. A novel enhanced feedback control strategy called ESOA-SME was introduced in this system to minimize the error of force estimation. The system (robotic hand with hard dynamics) along with the proposed control strategy was evaluated in MATLAB/SIMULINK platform. As a result, the proposed ESOA-SME model outperformed the existing models taken for comparison such as, SME, PSO-SME, and GA-SME, when evaluated for absolute error, MAE, MSE, and RMSE. The ranges of improvement exhibited by the proposed ESOA-SME were found to be 83.36%-97.29%, 83.48%-99.78%, and 75.98%-99.81%, for SME, PSO-SME, and GA-SME, respectively.

6. Funding and Conflicts of Interests

This project obtained funding from Women Scientist Scheme, Department of Science and Technology, New Delhi India under WOS-A scheme.

The authors have no competing interests to declare that are relevant to the content of this article.

REFERENCE

[1] Yanco, H. A., Norton, A., Ober,W., Shane, D., Skinner,A., & Vice, J. (2015).Analysis of human- robot interaction at the darpa robotics challenge trials. Journal of Field Robotics, 32(3), 420-444.

[2] Bajaj,N.M.,Spiers, A.J.,&Dollar,A.M.(2019). State oftheartinartificialwrists: A review of prosthetic and robotic wrist design. IEEE Transactions on Robotics, 35(1), 261-277.

[3] Lee, J. D., Li, W. C., Shen, J. H., & Chuang, C. W. (2018, April). Multi-robotic arms automated production line. In 2018 4th International Conference on Control, Automation and Robotics (ICCAR) (pp. 26-30). IEEE.

[4] Beasley, R. A. (2012).Medical robots: currentsystems and research directions. Journal of Robotics, 2012.

[5] Heung, K. H., Tong, R. K., Lau, A. T., & Li, Z. (2019). Robotic glove with soft-elastic composite actuators for assisting activities of daily living.Soft robotics, 6(2), 289-304.

[6] Malūkas, U., Maskeliūnas, R., Damaševičius, R., &Woźniak, M. (2018). Real timepathfindingforassistedlivingusingdeeplearning. J.Univers.Comput.Sci, 24(4), 475-487.
[7] Kang, B. B., Choi, H., Lee, H., & Cho, K. J. (2019). Exo-glove poly II: A polymer- based soft wearable robot for the hand with a tendon-driven actuation system. Soft robotics, 6(2), 214-227.
[8] Luneckas,M.,Luneckas,T.,Udris,D.,Plonis,D.,Maskeliūnas,R., &Damaševičius,
[9] R.(2019).Energy-efficientwalkingoverirregularterrain:Acaseofhexapodrobot.
[10] Ivanovas,A.,Ostreika,A.,Maskeliūnas,R.,Damaševičius,R.,Połap,D.,&Woźniak,
[11] M.(2018).Blockmatchingbasedobstacleavoidanceforunmanne daerialvehicle. In Artificial Intelligence and Soft Computing: 17th International Conference, ICAISC 2018, Zakopane, Poland, June 3-7, 2018, Proceedings, Part I 17 (pp. 58-69). Springer International Publishing.
[12] Sapaty,P.(2015).Militaryrobotics:latesttrendsandspatialgrasp solutions. InternationalJournalofAdvanced ResearchinArtificialIntelligence, 4(4), 9-18.
[13] Zhang, B., Xie, Y., Zhou, J., Wang, K., & Zhang, Z. (2020). State-of-the-art robotic grippers, grasping and control strategies, as well as their applications in agricultural robots: A review. Computers and Electronics in Agriculture, 177, 105694.
[14] Adenugba, F., Misra, S., Maskeliūnas, R., Damaševičius, R., &Kazanavičius, E.(2019). Smart irrigation system for environmentalsustainability in Africa:An Internet
[15] of Everything (IoE) approach. Mathematical biosciences and engineering, 16(5), 5490- 5503.
[16] Golan, Y., Shapiro, A., &Rimon, E. D. (2020). A variable-structure robot hand thatusestheenvironmenttoachievegeneralpurposegrasps. IEEERoboticsand Automation Letters, 5(3), 4804-4811.
[17] Homberg, B. S., Katzschmann, R. K., Dogar, M. R., & Rus, D. (2019). Robust proprioceptive grasping with a soft robot hand.Autonomous Robots, 43, 681-696.
[18] Ji, S. Q., Huang, M. B., & Huang, H. P. (2019). Robot intelligent grasp of unknown objects based on multi-sensor information. Sensors, 19(7), 1595.
[19] Kang, L., Seo, J. T., Kim, S. H., Kim, W. J., & Yi, B. J. (2019). Design and implementation of a multi-function gripper for grasping general objects. Applied Sciences, 9(24), 5266.
[20] Mu, L., Cui, G., Liu, Y.,Cui, Y., Fu,L., &Gejima, Y.(2020).Designandsimulation of an integrated end-effector for picking kiwifruit by robot. Information Processing in Agriculture, 7(1), 58-71.
[21] Neha, E., Suhaib, M., Asthana, S., & Mukherjee, S. (2020). Grasp analysis of a four- fingered robotic hand based on matlabsimmechanics. Journal of Computational & Applied Research in Mechanical Engineering (JCARME), 9(2), 169-182.
[22] Zhou, J., Chen, X., Chang, U., Pan, J., Wang, W., & Wang, Z. (2018, November). Intuitive control of humanoid soft-robotic hand BCL-13. In 2018 IEEE-RAS 18th International Conference on Humanoid Robots (Humanoids)(pp. 314-319). IEEE.
[23] Dimalexis, A., Pyrovetsi, M., &Sgardelis, S. (1997). Foraging ecology of the greyheron (Ardea cinerea), great egret (Ardea alba) and little egret (Egrettagarzetta) in response to habitat, at 2 Greek wetlands. Colonial waterbirds, 261-272.
[24] Wiggins, D. A. (1991). Foraging success and aggression in solitary and group-feeding Great Egrets (Casmerodius albus). Colonial Waterbirds, 176-179.
[25] Kent,D.M.(1986).Behavior,habitatuse,andfoodofthreeegretsin amarine habitat. Colonial Waterbirds, 25-30.
[26] Maccarone, A. D., Brzorad, J. N., & Stone, H. M. (2012). A telemetry-based study of Snowy Egret (Egrettathula) nest-activity patterns, food-provisioning rates and foraging energetics. Waterbirds, 35(3), 394-401.
[27] Yagiz, N., Ozbulur, V., Derdiyok, A., &Inanc, N. (1997). Sliding modes control of vehicle suspension systems. In Proceedings of the European Simulation Multi Conference, Istan

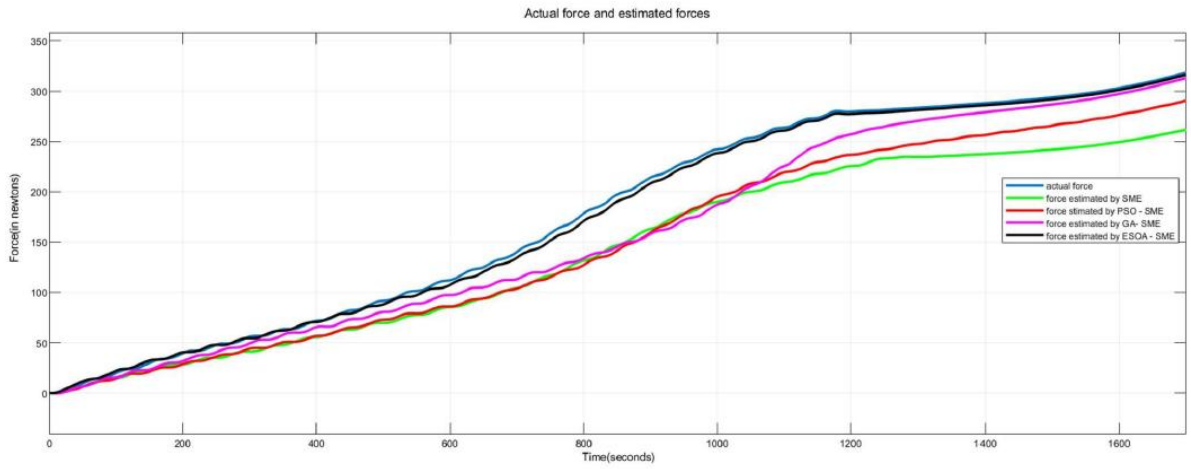


Figure7.ComparisonofForceEstimatedbyvariousSMEs

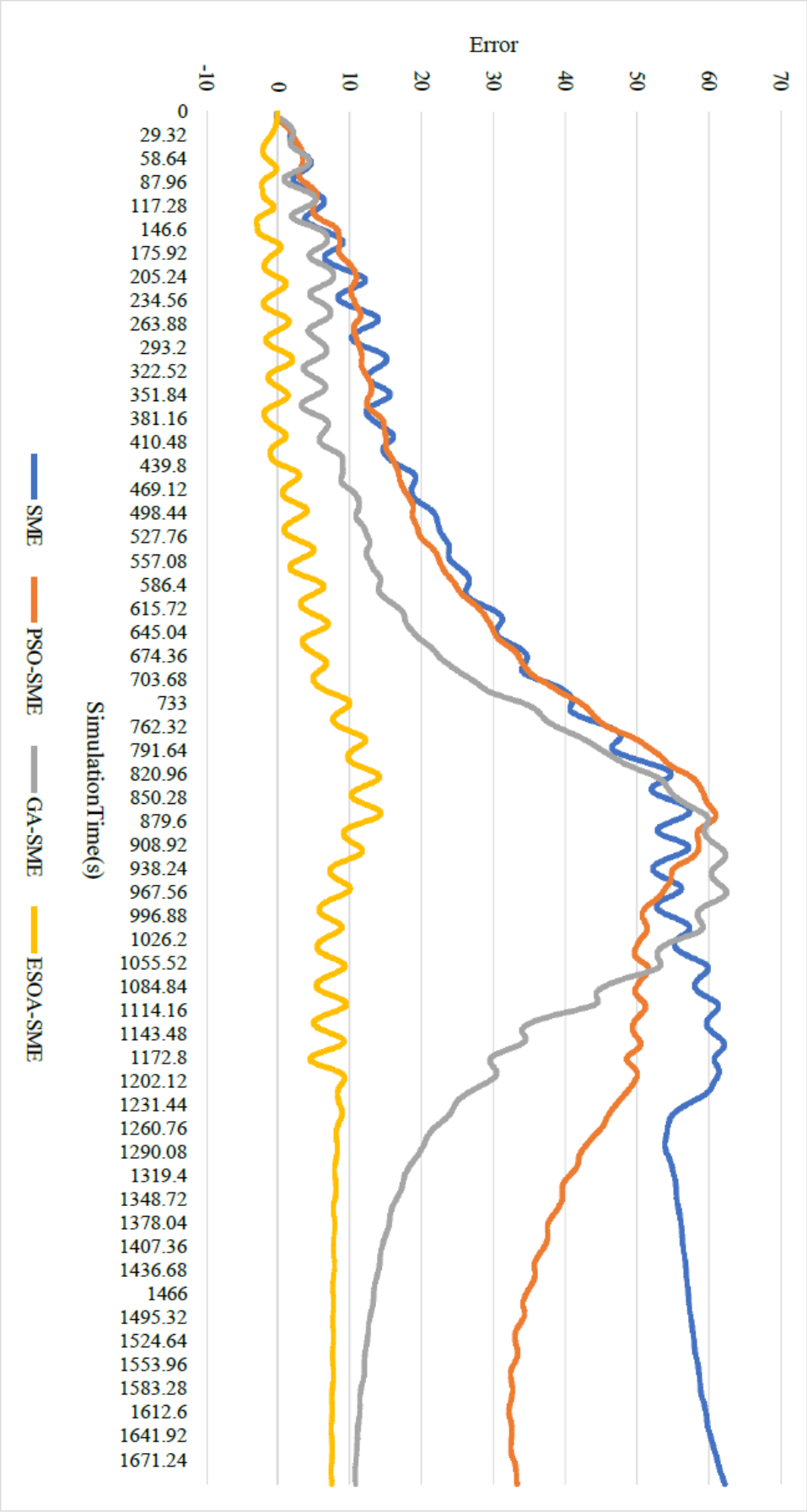


Figure8.ComparisonofAbsoluteErrorobtainedbyvariousSMEs

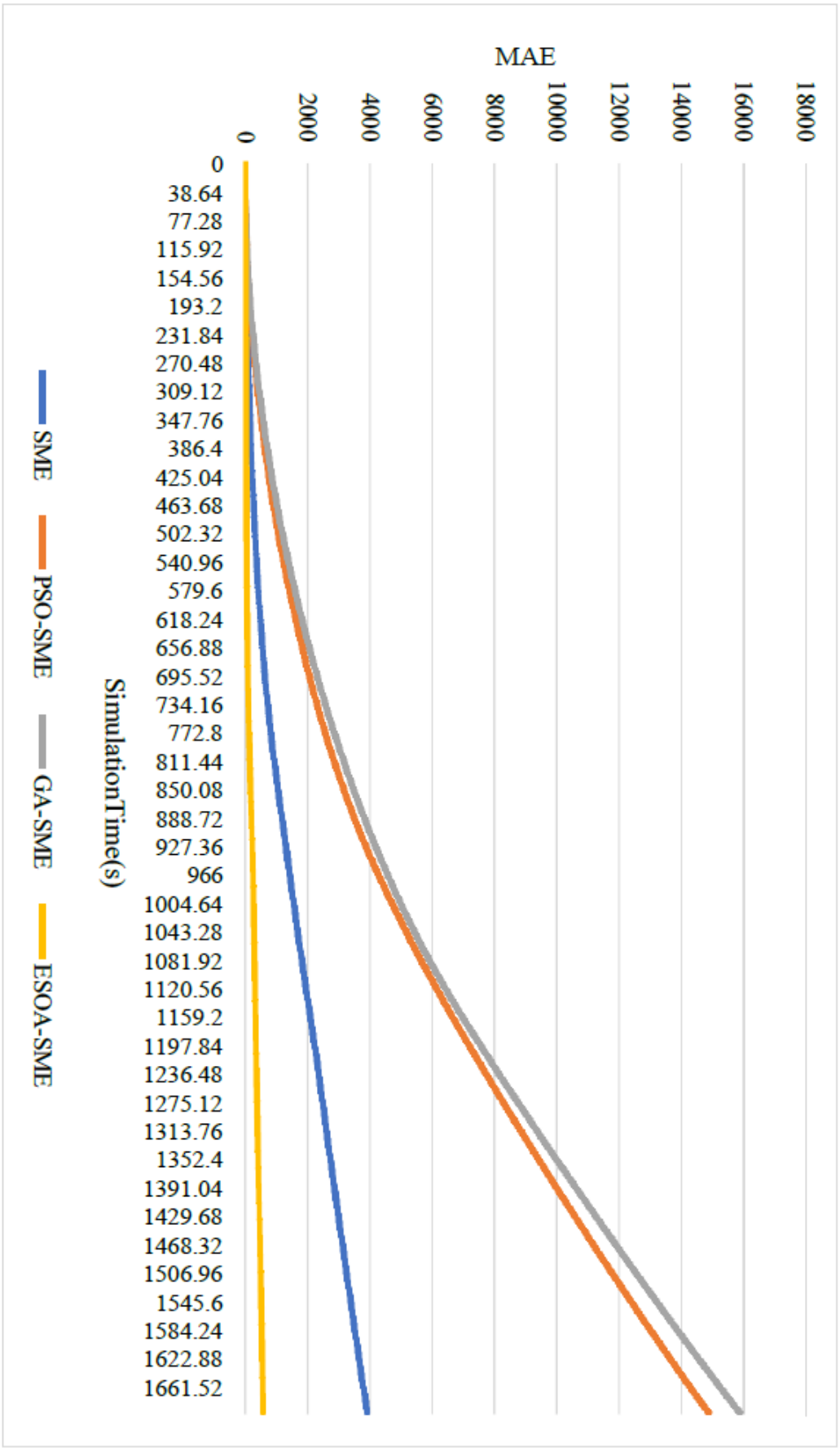


Figure9.ComparisonofMAEobtainedbyvariousSMEs

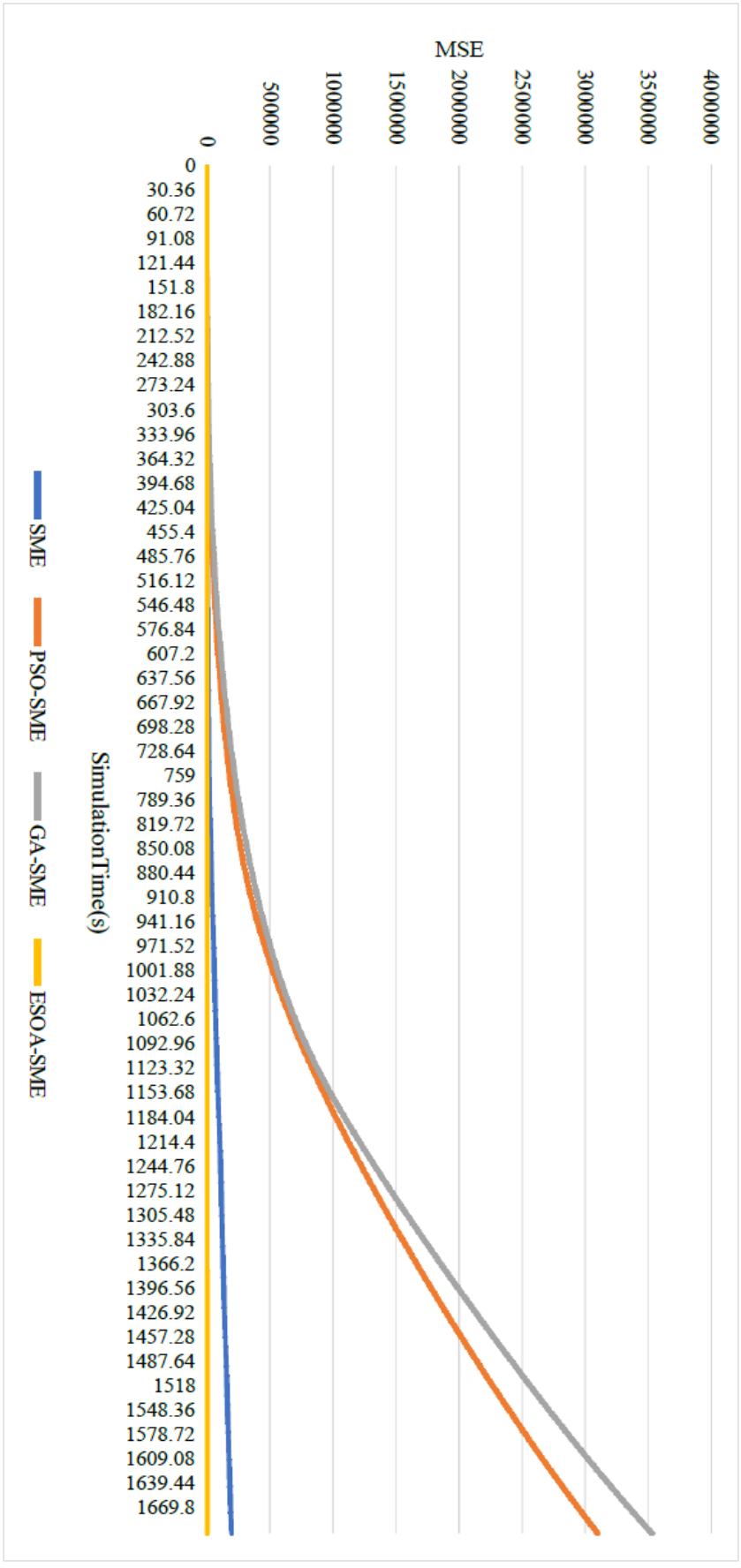


Figure10.ComparisonofMSEobtainedbyvariousSMEs

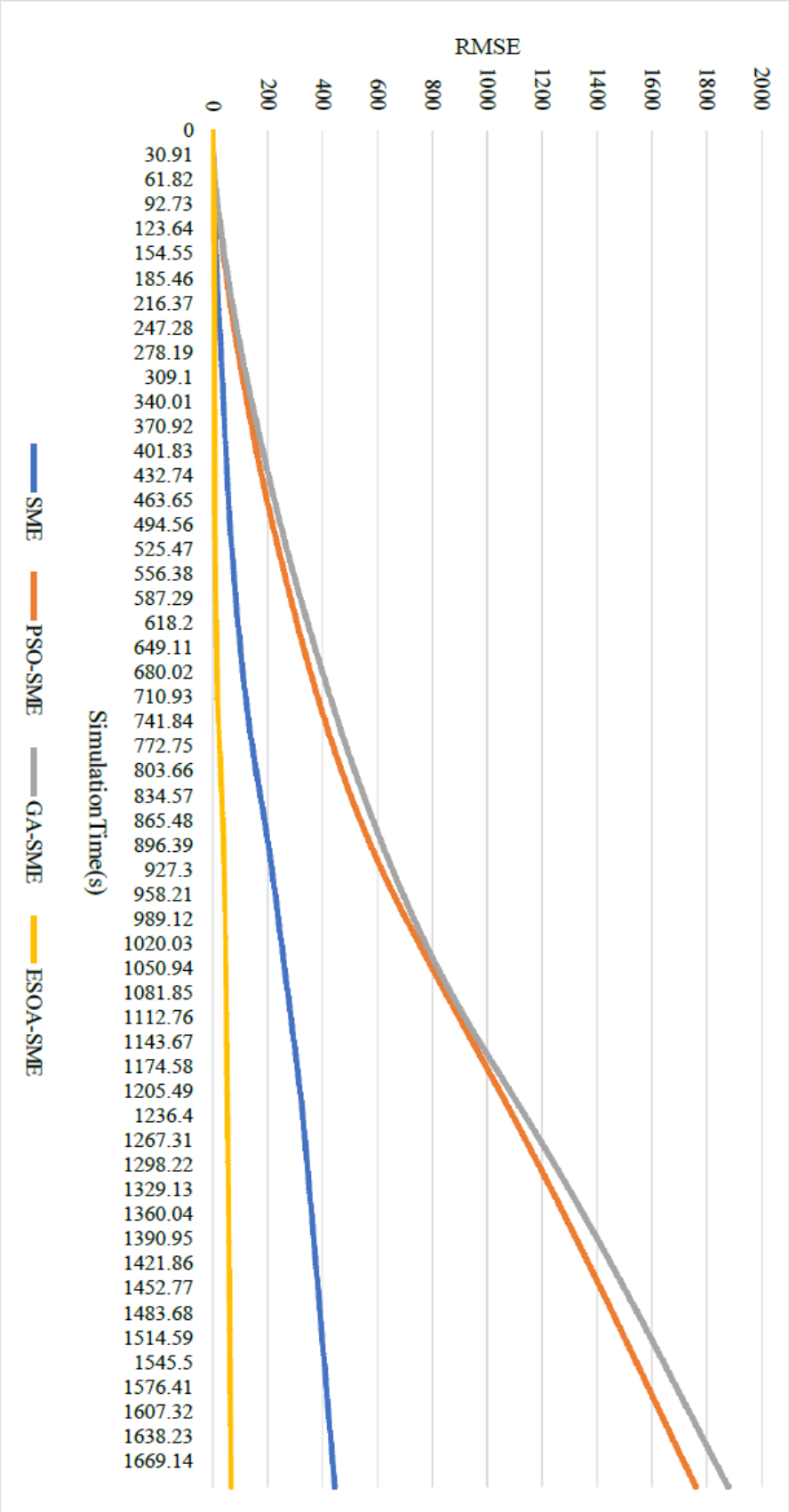


Figure11.ComparisonofRMSEobtainedbyvariousSMEs

★★★